


Article

Ultra-Wide-Bandwidth Tunable Magnetic Fluid-Filled Hybrid Connected Dual-Core Photonic Crystal Fiber Mode Converter

Yingying Yu and Bo Sun * 

Electronics and Information School, Yangtze University, Jingzhou 434000, China; yuyingying58@hotmail.com

* Correspondence: kylesunbo@hotmail.com

Received: 13 January 2018; Accepted: 10 February 2018; Published: 12 February 2018

Abstract: We propose a tunable magnetic fluid-filled hybrid photonic crystal fiber mode converter. Innovative design principles based on the hybrid connected dual-core photonic crystal fiber and magnetically modulated optical properties of magnetic fluid are developed and numerically verified. The mode converter was designed to convert LP_{11} in the index-guiding core to the LP_{01} mode in the photonic bandgap-guiding core. By introducing the magnetic fluid into the air-hole located at the center of the photonic bandgap-guiding core, the mode converter can realize a high coupling efficiency and an ultra-wide bandwidth. The coupling efficiency can reach up to 99.9%. At a fixed fiber length, by adjusting the strength of the magnetic field, the coupling efficiency can reach up to 90% and 95% at wavelengths in the ranges of $1.33\ \mu\text{m}$ – $1.85\ \mu\text{m}$ and $1.38\ \mu\text{m}$ – $1.75\ \mu\text{m}$, with bandwidth values reaching $0.52\ \mu\text{m}$ and $0.37\ \mu\text{m}$, respectively. Moreover, it has a good manufacturing flexibility. The mode converter can be used to implement wideband mode-division multiplexing of few-mode optical fiber for high-capacity telecommunications.

Keywords: mode converter; photonic crystal fiber; coupler; magnetic fluid; dual core fiber

1. Introduction

Since photonic crystal fiber (PCF) shows excellent optical properties, such as controllable birefringence, flexible dispersion, etc. [1–3], they have been receiving growing scientific and industrial interest [4–6]. Mounts for structures based on PCF have been designed, including index-guided PCFs [7], photonic bandgap fibers [8], hybrid PCFs [9], etc. Meanwhile, the multi-core PCF has also been extensively researched [10,11]. Multi-core PCF has excellent properties with regard to the coupling characteristics of the splitter, coupler and mode converter [12–15].

The mode converter is an important element in the mode-division multiplexing system [16–18]. Mode converters that convert several separate channels into the mode of few-mode fibers are essential components [19–21]. Bandwidth, dependent loss, and extinction ratio are important properties for mode-division systems. Integrated mode couplers based on silicon-on-insulator technology are suitable for high-performance mode converters [22,23]. Meanwhile, the PCF mode converter is also a promising solution for realizing a wide bandwidth, low dependent loss, and high extinction ratio. In other words, it is a promising candidate for a high-performance mode converter. Lai et al. constructed a PCF mode converter based on air-hole collapse [24]. Sun et al. have theoretically investigated the general principles of the PCF mode converter based on air-hole collapse [25]. Cai et al. proposed the tapered PCF and hybrid dual-core PCF mode converter to realize broadband and low-loss devices [26,27]. However, these mode converters still show relatively narrow bandwidth. Meanwhile, a tunable PCF mode converter has hardly been analyzed.

Magnetic fluid (MF) provides a viable solution for a tunable PCF mode converter. MF is a kind of magneto optical material that exhibits both fluidity, like liquid material, and magnetism, like solid

material [28]. The control mechanisms of MF in manipulating these optical properties have been studied by some institutions [29,30]. Based on the properties of MF, researches have been demonstrated their usefulness for magnetic field sensing, splitters, couplers, etc. [31–33]. However, the number of studies concerning mode converters based on MF has been relatively small.

In this paper, we propose a tunable MF-filled hybrid PCF mode converter. The bandwidth and the optimum operating wavelength are tunable by adjusting the strength of the magnetic field. The mode converter was designed to convert LP_{11} to the LP_{01} mode. The calculation is based on a finite difference beam propagation method (BPM), and a numerical calculation is carried out on this mode converter to determine the parameters that affect the mode conversion. The performance of such a mode converter is expected to be insensitive to parameters. Moreover, PCF postprocessing technique has been given considerable attention by the research workers in the past. Therefore, it is relatively easy to manipulate, and has been used to fabricate such a mode converter.

2. Structure of Magnetic Fluid-Filled Hybrid Photonic Crystal Fiber

As shown in Figure 1, the MF-filled hybrid PCF has the following variable parameters: $\Lambda = 6 \mu\text{m}$, $D_1 = 5.4 \mu\text{m}$, $D_2 = 3 \mu\text{m}$, and $D_3 = 1.5 \mu\text{m}$, where Λ is the air-hole pitch, D_1 , D_2 , and D_3 are the normal, compressed, and filled air-hole diameters, respectively. Background silica index is assumed to be 1.45. The red circle hole located at the center of core B, is filled with MF. In contrast to traditional PCF, the structure has a connected dual core (A and B), and shares properties of both the photonic bandgap (PBG)-guiding and the index-guiding mechanisms. The operation of the proposed hybrid PCF mode converter is based on power transfer between the PBG-guiding core (core B) and the index-guiding core (core A) mode. The gradual crossover of propagation constants between the two modes leads to the power transfer. The hybrid PCF mode converter is employed to support a fundamental mode LP_{01} and a second-order mode LP_{11} . A LP_{11} mode is ported into the core A of the MF-filled hybrid PCF at the input side by offset splicing with a piece of multimode fiber. At the output side, a standard SMF is spliced to the hybrid PCF for exciting the LP_{01} mode purely in core B.

The refractive index of MF can be changed with an applied external magnetic field. When the magnetic field strength exceeds a critical value, the refractive index increases with the rising magnetic field strength, reaching a saturated value under a higher strength. The variation in refractive index of MF with the field strength H and the temperature T is attributed to the column formation, the trend of the refractive index of MF should be similar to Langevin function. The refractive index of MF is described in detail [28,31]:

$$RI_{MF}(H, T) = [n_s - n_o] \left[\coth\left(a \frac{H - H_{c,n}}{T}\right) - \frac{T}{a(H - H_{c,n})} \right] + n_o, \text{ for } H > H_{c,n} \quad (1)$$

where n_o ($=1.4620$ here) is the refractive index of MF under magnetic field lower than $H_{c,n}$ (critical field strength). n_s ($=1.4704$ here) is the saturated value of the refractive index of MF. a is the fitting parameter, H is the field strength in Oe, and T is the temperature in Kelvin. In this paper, the temperature is set to be $24.3^\circ\text{C} = 397.45^\circ\text{K}$, $H_{c,n}$ is 30 Oe, and a is 3.01. At 24.3°C , the refractive index of MF as a function of the magnetic field strength is shown in Figure 2.

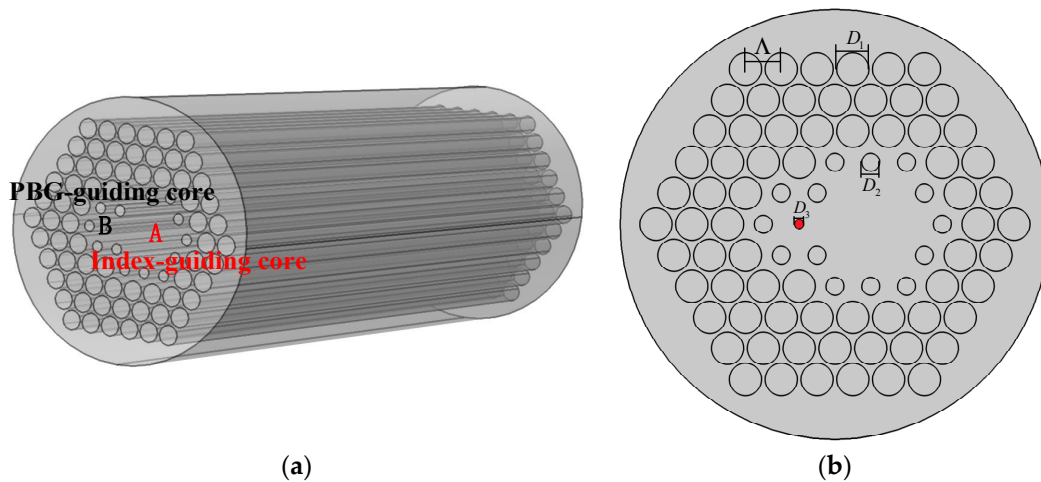


Figure 1. (a) Schematic of magnetic fluid-filled hybrid PCF; (b) Cross section of the proposed PCF.

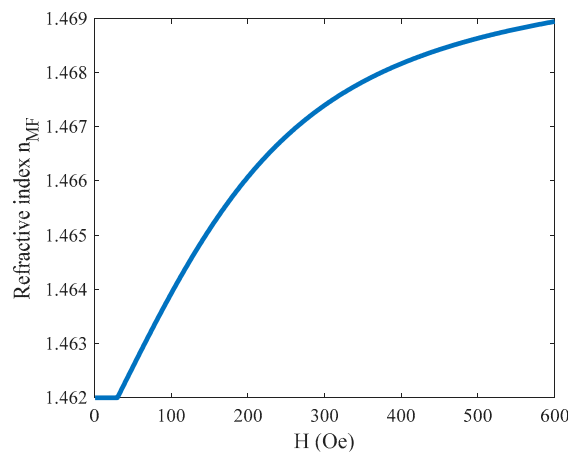


Figure 2. Refractive index of MF as a function of the magnetic field strength.

3. Numerical Analysis and Simulated Results

In the calculation, the temperature is 24.3 °C, $H = 73$ Oe, and the refractive index of MF $RI_{MF} = 1.4632$. Combined with the BPM, when a LP_{11} mode is ported into core A, Figure 3 shows the coupling efficiency of the MF-filled hybrid PCF at the fixed fiber length $Z = 835 \mu\text{m}$, and the effective refractive index of the LP_{11} mode in core A and the LP_{01} mode in core B. From the figure, we can see that when the wavelength $\lambda = 1.55 \mu\text{m}$, the coupling efficiency is maximized, and the optical power is coupled with core B. Core A is treated as an independent waveguide, which is affected by the perturbation of light waves traveling in core B. When the effective refractive indexes of the LP_{11} mode and the LP_{01} mode in the individual cores are equal, the phase matching condition is satisfied, which enables the coupling between core A and core B. From the figure, we can see that the phase matching wavelength is at approximately $1.532 \mu\text{m}$. There is a small difference between $1.532 \mu\text{m}$ and $1.55 \mu\text{m}$, because the refractive indexes are obtained in single-core situation without considering the impact of a connected dual core. In addition, the hybrid PCF mode converter exhibits an ultra-wide bandwidth. The coupling efficiency can reach up to 90% and 95% at wavelength ranges of $1.378 \mu\text{m}$ – $1.736 \mu\text{m}$ and $1.423 \mu\text{m}$ – $1.678 \mu\text{m}$, where the maximum bandwidth value can reach $0.358 \mu\text{m}$ and $0.255 \mu\text{m}$, respectively. The wide bandwidth mode conversion is due to the small differences in the propagation constants of the two modes in the long-wavelength range. When $\lambda = 1.4 \mu\text{m}$ and $\lambda = 1.7 \mu\text{m}$, the effective refractive index differences between the LP_{11} mode and the LP_{01} mode are only 2.63×10^{-4} and 3.76×10^{-4} , respectively.

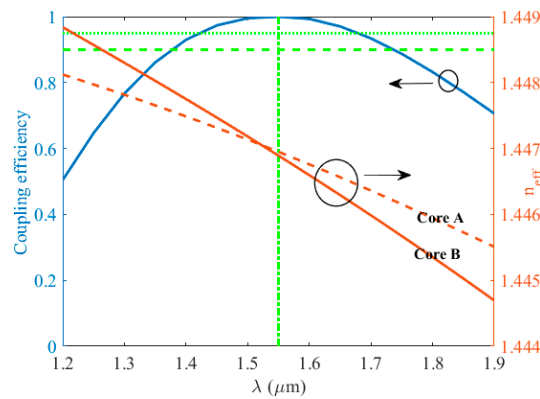


Figure 3. Coupling efficiency of the MF-filled hybrid PCF, and effective refractive index of the LP₁₁ mode in core A and the LP₀₁ mode in core B.

To further analyze the coupling characteristics, the calculated mode field distribution of the mode converter is discussed. Figure 4 shows the process of mode conversion between the LP₁₁ and LP₀₁ mode along the propagation direction at the coupling length $Z = L_c$, the operating wavelength is 1.55 μm . From Figure 4, we can see that the input light of LP₁₁ mode is almost completely coupled into LP₀₁ mode, and the coupling efficiency can reach up to 99.9% at $Z = L_c/2 = 853 \mu\text{m}$. The calculated mode field distribution of the mode converter is also shown for different wavelengths. Figure 5 shows that the mode field distributions at the fixed fiber length is 835 μm for different wavelengths. From the figure, we can see that the coupling efficiency of mode converter can reach up to 76.7%, 90.6%, 90.3%, and 82.7% at $\lambda = 1.3 \mu\text{m}$, $\lambda = 1.38 \mu\text{m}$, $\lambda = 1.73 \mu\text{m}$, and $\lambda = 1.8 \mu\text{m}$, respectively.

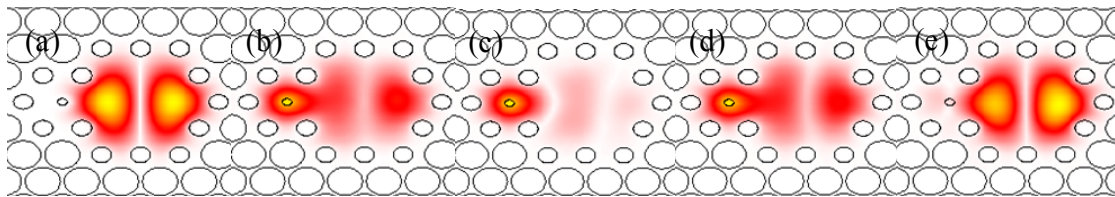


Figure 4. Power transfer from the index-guiding to the PGB core at propagating distance (a) $Z = 0$; (b) $Z = L_c/4$; (c) $Z = L_c/2$; (d) $Z = 3L_c/4$; and (e) $Z = L_c$. The coupling length is $L_c = 1670 \mu\text{m}$, the operating wavelength is 1.55 μm .

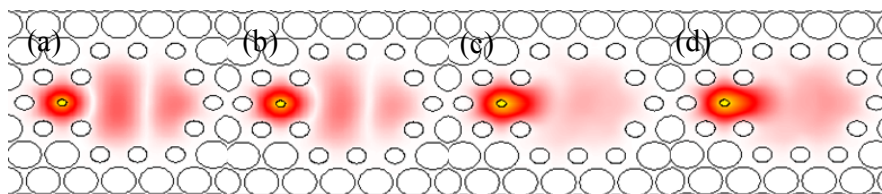


Figure 5. Mode field distribution of the mode converter at (a) $\lambda = 1.3 \mu\text{m}$; (b) $\lambda = 1.38 \mu\text{m}$; (c) $\lambda = 1.73 \mu\text{m}$; and (d) $\lambda = 1.8 \mu\text{m}$.

From Equation (1), we know that the refractive index of MF varies with magnetic field strength. The coupling characteristics can be controlled by changing the magnetic field strength. We can further increase the bandwidth and change the optimum operating wavelength of the mode converter. Figure 6a shows the coupling efficiency of the mode conversion for different refractive indexes of MF at $Z = 835 \mu\text{m}$. From the figure, we can see that the coupling efficiency can reach up to 90% in the wavelength range of 1.33 μm –1.85 μm , and the maximum bandwidth value can reach 0.52 μm . Moreover, the coupling efficiency can reach up to 95% in the wavelength range of 1.38 μm –1.75 μm , the maximum bandwidth value can reach 0.37 μm . By changing the magnetic

field strength, the bandwidth is further increased. The comparison among the properties of the tunable MF-filled hybrid PCF mode converter with existing structures in the literature is shown in Table 1. The performance comparison has taken into account structure type, coupling efficiency at 1.55 μm , and bandwidth range. As is clearly evident from the table, the proposed mode converter shows better performance in terms of high coupling efficiency and wide bandwidth.

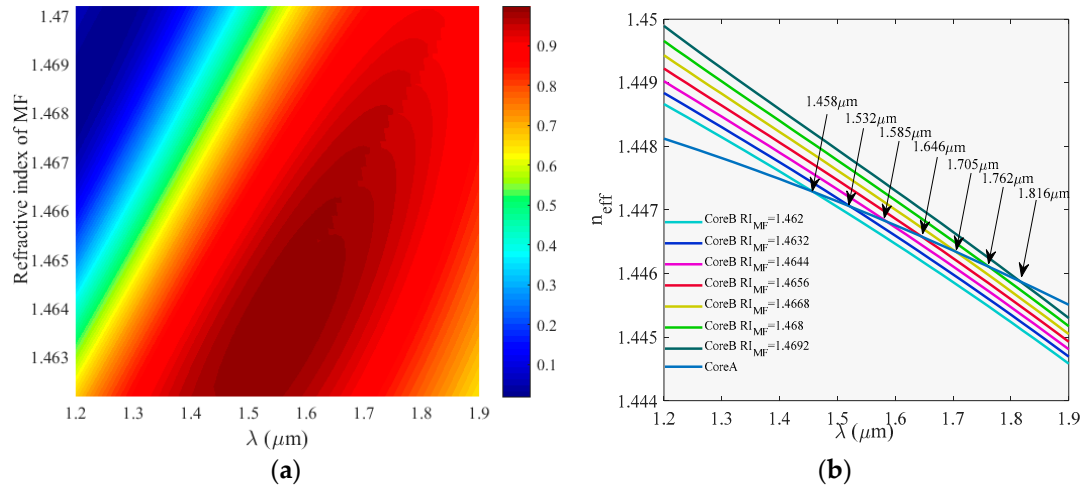


Figure 6. (a) Coupling efficiency of the MF-filled hybrid PCF for different refractive index of MF at the fixed fiber length $Z = 835 \mu\text{m}$; (b) Effective refractive index of the LP_{11} mode in core A and the LP_{01} mode in core B at different refractive indexes of MF.

Table 1. Comparison among the properties of the proposed fiber with previously reported mode converter.

References	Structure Type	Coupling Efficiency	Bandwidth Range
[20]	Multi-plane	94%	1530 nm–1565 nm
[23]	SOI-based rib waveguide	97.5%	1500 nm–1600 nm
[26]	Dual-core PCF	95%	1460 nm–1625 nm
[34]	Tapered Mode	99%	1527 nm–1620 nm
[35]	Polymer Waveguide Grating	99%	1530 nm–1625 nm
This work	MF-filled hybrid PCF	99.9%	1380 nm–1750 nm

Meanwhile, with the increase of the refractive index of MF, the optimum operating wavelength shifts to a longer wavelength. To further numerically analyze the coupling performance, Figure 6b shows the effective refractive index of the LP_{11} mode in core A and the LP_{01} mode in core B at different refractive index of MF. At the wavelengths corresponding to the intersection points, the LP_{11} mode and the LP_{01} mode have the same mode refractive index. The intersection points suggest the wavelengths where the LP_{11} mode is coupled into LP_{01} mode. The figure shows a qualitative understanding of our structure. From the figure, we can see that with the increase of the refractive index of the MF, the phase matching wavelength shifts from 1.458 μm to 1.816 μm . This result could indicate that when the refractive index of MF increases, the effective refractive index curve of the LP_{11} mode does not change, but the effective refractive index curve of the LP_{01} mode shifts up due to the increase of the refractive index of MF. Furthermore, the ultra-wide bandwidth mode conversion is due to the small differences of the propagation constants of the two modes in the long-wavelength range. We can further decrease the effective refractive index difference by changing the refractive index of MF, and that which results in the increase of coupling strength. For example, when the operating wavelength is 1.3 μm , the effective refractive index difference between the LP_{11} mode and the LP_{01} mode is 3.64×10^{-4} at $RI_{\text{MF}} = 1.462$, and further increase the coupling efficiency at $\lambda = 1.3 \mu\text{m}$. Figure 7 shows the mode field distribution of the mode converter at $Z = 835 \mu\text{m}$ for different magnetic field strength. From the figure, we can

see that the coupling efficiency is up to 86.9%, 95.8%, 96.2%, and 92.9% at $\lambda = 1.3 \mu\text{m}$, $\lambda = 1.38 \mu\text{m}$, $\lambda = 1.73 \mu\text{m}$, and $\lambda = 1.8 \mu\text{m}$, respectively. Compared with the Figure 5, the coupling efficiency is significantly increased due to the change of magnetic field strength.

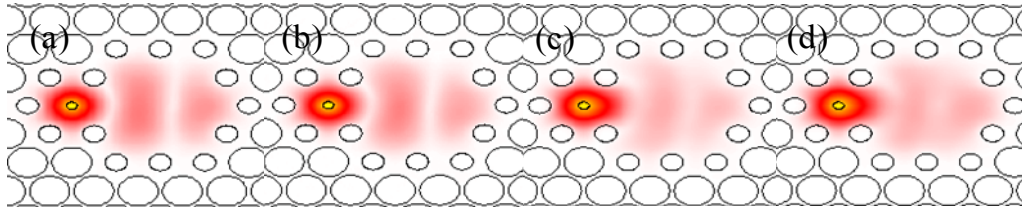


Figure 7. Mode field distribution of the mode converter at (a) $\lambda = 1.3 \mu\text{m}$, $RI_{MF} = 1.462$ ($H < 30$); (b) $\lambda = 1.38 \mu\text{m}$, $RI_{MF} = 1.462$ ($H < 30$); (c) $\lambda = 1.73 \mu\text{m}$, $RI_{MF} = 1.466$ ($H = 198$); and (d) $\lambda = 1.8 \mu\text{m}$, $RI_{MF} = 1.4672$ ($H = 282$).

The air-hole diameter D_3 is the crucial parameter, and it affects the coupling characteristics. Figure 8 shows the effect of the D_3 on coupling characteristics. From the Figure 8a, we can find that the coupling strength first increases and then rapidly decreases with the increase of D_3 , for the reason that, with the increase of D_3 , the effective refractive index curve of core B is characterized by its exponential shape, but the effective refractive index curve of core A only changes slightly. The difference in the propagation constants of the two cores first decreases and then rapidly increases, resulting in the rapid decrease of coupling strength at larger D_3 . Therefore, in order to achieve efficient mode conversion, a particular value of D_3 is needed. Taking into account the actual fabrication process, the structural accuracy may be influenced by the nonuniformity of the device itself. To further analyze the geometrical errors, we define the power difference (PD) of core A and core B, PD as [32,36]:

$$PD = 10 \log_{10} \frac{P_{coreA}}{P_{coreB}} \quad (2)$$

where P_{coreA} and P_{coreB} are the output power of core A and core B, respectively. The fabrication flexibility is discussed as shown in Figure 9. When the operating wavelength is $1.55 \mu\text{m}$, the PD can reach up to -35 dB and -40 dB for D_2 , with a structural deviation of $\pm 0.5\%$, and the PD can also reach up to -33 dB and -50 dB for D_3 , with a structural deviation of $\pm 0.5\%$, which indicates that LP_{11} mode can be completely coupled into LP_{01} mode, regardless of the structural inaccuracy. The mode conversion can operate well within an error of 0.5% . Meanwhile, structural inaccuracy does not cause a change in bandwidth.

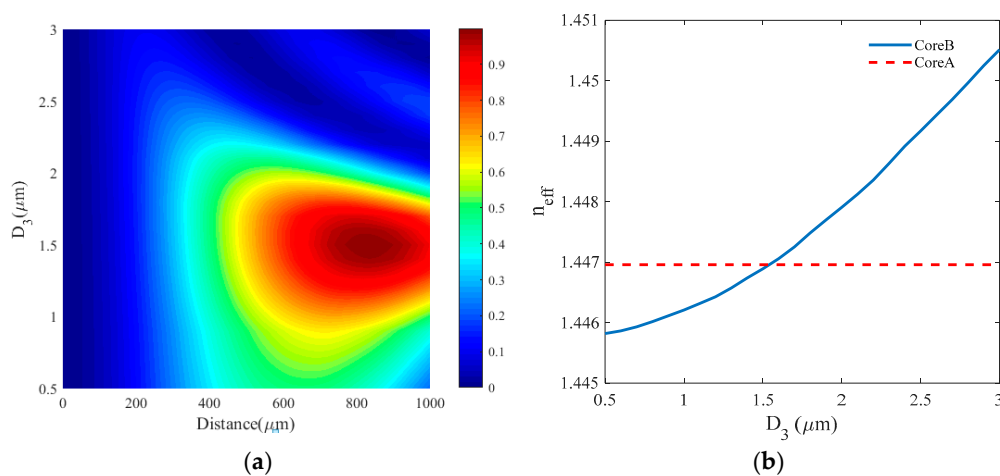


Figure 8. (a) Coefficient efficiency of the MF-filled hybrid PCF for different D_3 at $\lambda = 1.55 \mu\text{m}$; (b) Effective refractive index of the LP_{11} mode in core A and the LP_{01} mode in core B for different D_3 .

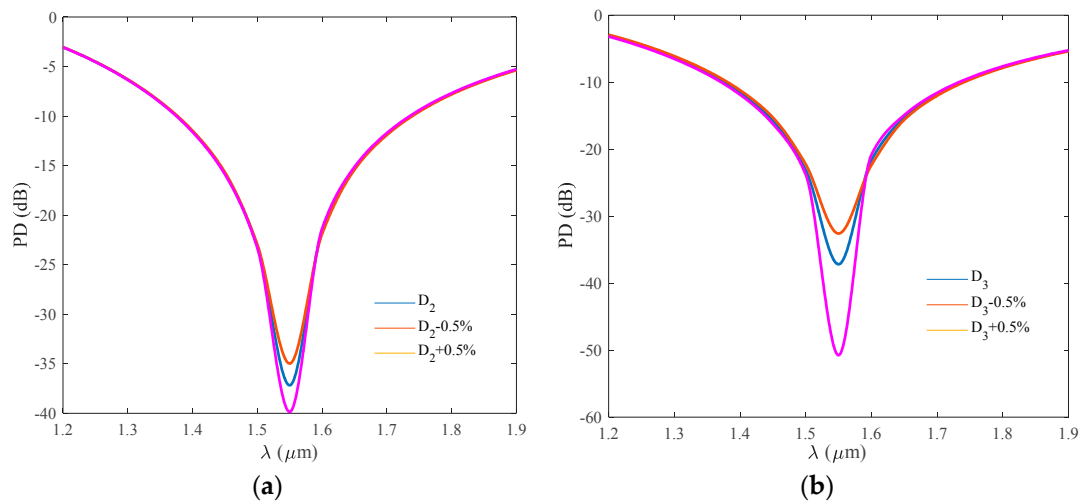


Figure 9. PD versus the wavelength at various fabrication tolerances. (a) D_2 with a fabrication tolerance of 0.5%; (b) D_3 with a fabrication tolerance of 0.5%.

All the above results are based on a fixed fiber length. By changing the fiber length, we can achieve a high coupling efficiency at a longer wavelength. Figure 10a shows the coupling efficiency for long wavelengths as a function of distance. From the figure, we can see that the coupling efficiency can be significantly increased by changing the fiber length. Because the coupling length is decreased with the increase of wavelength, the coupling length is inversely proportional to wavelength. The coupling efficiency can also reach up to 99.8%, 99.2%, and 97.7% at $\lambda = 1.55 \mu\text{m}$, $\lambda = 2.0 \mu\text{m}$, and $\lambda = 2.1 \mu\text{m}$, respectively. Although the fiber length affects the coupling efficiency, the mode conversion can also operate well within an error of 0.5%. The fabrication flexibility of fiber length is discussed as shown in Figure 10b. From the figure, we can see that when $\lambda = 1.55 \mu\text{m}$, and $Z = 835 \mu\text{m}$, the mode conversion shows good stability within an error of 0.5%.

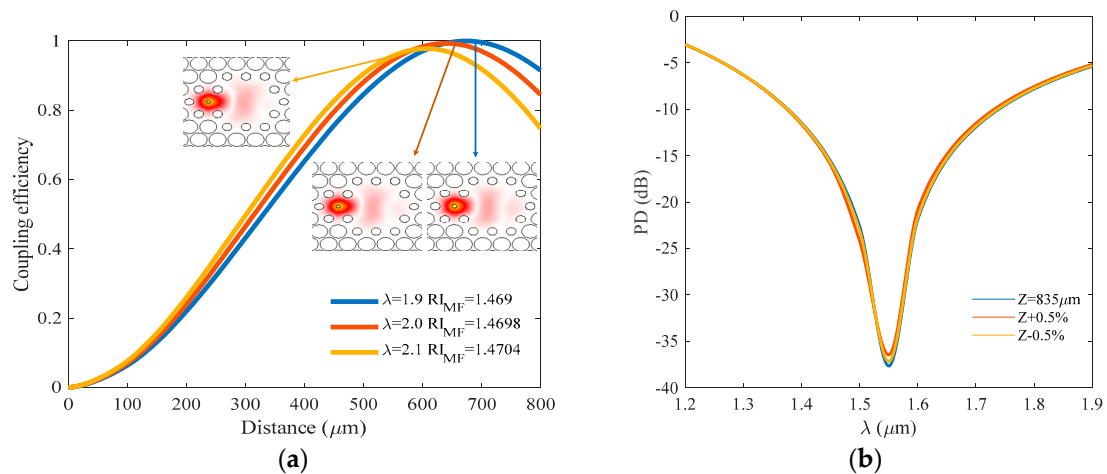


Figure 10. (a) Coupling efficiency as a function of distance for different long wavelengths; (b) PD versus the wavelength at fiber length with a fabrication tolerance of 0.5%.

In addition, the structural accuracy is also influenced by the environment. According to the results discussed above, we know that in order to achieve a higher coupling efficiency, a particular value of refractive index of the MF is needed. However, from Equation (1), we know that the refractive index of MF varies with temperature. The temperature can affect the coupling efficiency and bandwidth. In the temperature range of 0–55 $^{\circ}\text{C}$, magnetic strength has a linear relation to the temperature [27,31]. Therefore, at different temperatures, higher coupling efficiency can be realized by adjusting the

magnetic field strength. Based on the above, these error tolerances are experimentally feasible and realistic.

4. Conclusions

In conclusion, a MF-filled hybrid PCF mode converter has been presented. The design is based on a connected dual-core PCF, and shares properties of both the PBG-guiding and the index-guiding mechanisms. The PCF is filled with MF in the PBG-guiding core, whose refractive index varies with the magnetic field strength, and realizes a tunable mode converter. Study results demonstrate that the mode converter shows a high coupling efficiency and an ultra-wide bandwidth. Meanwhile, by changing the magnetic field strength, the bandwidth can be further increased, and the optimum operating wavelength can be changed. At a fixed fiber length, by adjusting the strength of magnetic field, the coupling efficiency can reach up to 90% and 95% at wavelength ranges of 1.33 μm –1.85 μm and 1.38 μm –1.75 μm , while the bandwidth value can reach 0.52 μm and 0.37 μm , respectively. Additionally, the designed MF-filled hybrid PCF mode converter has good manufacturing flexibility. Therefore, the mode converter works well with a fabrication tolerance of 0.5%. The mode converter can be used to implement wideband mode-division multiplexing of few-mode optical fiber for high capacity telecommunications.

Acknowledgments: This work is supported by the National Natural Science Foundation of China (Grant 51309059), and Electric & Information School of Yangtze University Innovation Foundation (Grant 2016-DXCX-02 and Grant 2016-DXCX-04).

Author Contributions: Yingying Yu performed the simulations and helped check the scientific content the manuscript. Bo Sun supervised the whole study and finalized the manuscript.

Conflicts of Interest: The authors declare no conflict of interest.

References

1. Peyrilloux, A.; Chartier, T.; Hideur, A.; Berthelot, L. Theoretical and Experimental Study of the Birefringence of a Photonic Crystal Fiber. *J. Lightwave Technol.* **2016**, *21*, 536–539. [[CrossRef](#)]
2. Islam, M.A.; Alam, M.S. Design Optimization of Equiangular Spiral Photonic Crystal Fiber for Large Negative Flat Dispersion and High Birefringence. *J. Lightwave Technol.* **2012**, *30*, 3545–3551. [[CrossRef](#)]
3. Saitoh, K.; Florous, N.; Koshiba, M. Ultra-flattened chromatic dispersion controllability using a defected-core photonic crystal fiber with low confinement losses. *Opt. Express* **2005**, *13*, 8365–8371. [[CrossRef](#)] [[PubMed](#)]
4. Rifat, A.A.; Mahdiraji, G.A.; Ahmed, R.; Chow, M.D.; Sua, Y.M.; Shee, Y.G.; Adikan, F.R.M. Copper-Graphene-Based Photonic Crystal Fiber Plasmonic Biosensor. *IEEE Photonics J.* **2017**, *8*, 1–8. [[CrossRef](#)]
5. Vigneswaran, D.; Ayyanar, N.; Sharma, M.; Maburajan, M.S.; Porsezian, K. Salinity sensor using photonic crystal fiber. *Sens. Actuators A Phys.* **2018**, *269*, 22–28. [[CrossRef](#)]
6. Ahmed, K.; Morshed, M. Design and numerical analysis of microstructured-core octagonal photonic crystal fiber for sensing applications. *Sens. Bio-Sens. Res.* **2016**, *7*, 1–6. [[CrossRef](#)]
7. Zhang, Z.G.; Zhang, F.D.; Zhang, M.; Ye, P.D. Gas sensing properties of index-guided PCF with air-core. *Opt. Laser Technol.* **2008**, *40*, 167–174.
8. Saitoh, K.; Koshiba, M. Leakage loss and group velocity dispersion in air-core photonic bandgap fibers. *Opt. Express* **2003**, *11*, 3100–3109. [[CrossRef](#)] [[PubMed](#)]
9. Asaduzzaman, S.; Ahmed, K.; Bhuiyan, T.; Farah, T. Hybrid photonic crystal fiber in chemical sensing. *Springerplus* **2016**, *5*, 1–11. [[CrossRef](#)] [[PubMed](#)]
10. Saitoh, K.; Sato, Y.; Koshiba, M. Coupling characteristics of dual-core photonic crystal fiber couplers. *Opt. Express* **2003**, *11*, 3188–3195. [[CrossRef](#)] [[PubMed](#)]
11. Liu, S.; Li, S.G.; Yin, G.B.; Feng, R.P.; Wang, X.Y. A novel polarization splitter in ZnTe tellurite glass three-core photonic crystal fiber. *Opt. Commun.* **2012**, *285*, 1097–1102. [[CrossRef](#)]
12. Zhao, T.; Lou, S.; Wang, X.; Zhou, M.; Lian, Z. Ultrabroadband polarization splitter based on three-core photonic crystal fiber with a modulation core. *Appl. Opt.* **2016**, *55*, 6428–6434. [[CrossRef](#)] [[PubMed](#)]
13. Kim, H.; Kim, J.; Paek, U.C.; Lee, B.H.; Kim, K.T. Tunable photonic crystal fiber coupler based on a side-polishing technique. *Opt. Lett.* **2004**, *29*, 1194–1196. [[CrossRef](#)] [[PubMed](#)]

14. Nandi, P.; Chen, Z.; Witkowska, A.; Wadsworth, W.J.; Birks, T.A.; Knight, J.C. Characterization of a photonic crystal fiber mode converter using low coherence interferometry. *Opt. Lett.* **2009**, *34*, 1123–1125. [[CrossRef](#)] [[PubMed](#)]
15. Hu, D.J.; Ping, S.; Lu, C.; Sun, X.; Ren, G.; Yu, X.; Wang, G. Design and analysis of thermally tunable liquid crystal filled hybrid photonic crystal fiber coupler. *Opt. Commun.* **2009**, *282*, 2343–2347. [[CrossRef](#)]
16. Richardson, D.J.; Fini, J.M.; Nelson, L.E. Space-division multiplexing in optical fibres. *Nat. Photonics* **2013**, *7*, 354–362. [[CrossRef](#)]
17. Leon-Saval, S.G.; Fontaine, N.K.; Amezcua-Correa, R. Photonic lantern as mode multiplexer for multimode optical communications. *Opt. Fiber Technol.* **2017**, *35*, 46–55. [[CrossRef](#)]
18. Leon-Saval, S.G.; Fontaine, N.K.; Salazar-Gil, J.R.; Ercan, B.; Ryf, R.; Bland-Hawthorn, J. Mode-selective photonic lanterns for space-division multiplexing. *Opt. Express* **2014**, *22*, 1036–1044. [[CrossRef](#)] [[PubMed](#)]
19. Velazquez-Benitez, A.M.; Alvarado, J.C.; Lopez-Galmiche, G.; Antonio-Lopez, J.E.; Hernández-Cordero, J.; Sanchez-Mondragon, J.; Sillard, P.; Okonkwo, C.M.; Amezcua-Correa, R. Six mode selective fiber optic spatial multiplexer. *Opt. Lett.* **2015**, *40*, 1663–1666. [[CrossRef](#)] [[PubMed](#)]
20. Labroille, G.; Denolle, B.; Jian, P.; Genevaux, P.; Treps, N.; Morizur, J.F. Efficient and mode selective spatial mode multiplexer based on multi-plane light conversion. *Opt. Express* **2014**, *22*, 15599–15607. [[CrossRef](#)] [[PubMed](#)]
21. Shwartz, S.; Golub, M.A.; Ruschin, S. Computer-generated holograms for fiber optical communication with spatial-division multiplexing. *Appl. Opt.* **2017**, *56*, A31–A40. [[CrossRef](#)]
22. Chen, H.; Sleiffer, V.; Snyder, B.; Kuschnerov, M.; Vanuden, R.; Jung, Y.; Okonkwo, C.M.; Raz, O.; Brien, P.O.; Waardt, H.D.; et al. Demonstration of a Photonic Integrated Mode Coupler With MDM and WDM Transmission. *IEEE Photonics Technol. Lett.* **2013**, *25*, 2039–2042. [[CrossRef](#)]
23. Xing, J.J.; Li, Z.Y.; Xiao, X.; Yu, J.Z.; Yu, Y.D. Two-mode multiplexer and demultiplexer based on adiabatic couplers. *Opt. Lett.* **2013**, *38*, 3468–3470. [[CrossRef](#)] [[PubMed](#)]
24. Lai, K.; Leonsaval, S.G.; Witkowska, A.; Wadsworth, W.J.; Briks, T.A. Wavelength-independent all-fiber mode converters. *Opt. Lett.* **2007**, *32*, 328–330. [[CrossRef](#)] [[PubMed](#)]
25. Sun, G.L.; Chen, Z.L.; Xi, X.M.; Hou, J.; Jiang, Z.F. General principles for designing mode converters based on air-hole collapse in photonic crystal fibers. *Opt. Commun.* **2012**, *285*, 1331–1334.
26. Cai, S.; Yu, S.; Lan, M.; Gao, L.; Nie, S.; Gu, W. Broadband Mode Converter Based on Photonic Crystal Fiber. *IEEE Photonics Technol. Lett.* **2015**, *27*, 474–477. [[CrossRef](#)]
27. Cai, S.; Yu, S.; Wang, Y.; Lan, M.; Gao, L.; Gu, W. Hybrid Dual-Core Photonic Crystal Fiber for Spatial Mode Conversion. *IEEE Photonics Technol. Lett.* **2016**, *28*, 339–342. [[CrossRef](#)]
28. Chen, Y.F.; Yang, S.Y.; Tse, W.S.; Horng, H.E.; Hong, C.; Yang, H.C. Thermal effect on the field-dependent refractive index of the magnetic fluid film. *Appl. Phys. Lett.* **2003**, *82*, 3481–3483. [[CrossRef](#)]
29. Horng, H.E.; Chieh, J.J.; Chao, Y.H.; Yang, S.Y.; Hong, C.Y.; Yang, H.C. Designing optical-fiber modulators by using magnetic fluids. *Opt. Lett.* **2005**, *30*, 543–545. [[CrossRef](#)] [[PubMed](#)]
30. Otmani, H.; Bouchemat, M.; Bouchemat, T.; Lahoubi, M.; Wang, W.; Pu, S. Nonreciprocal TE–TM Mode Conversion Based on Photonic Crystal Fiber of Air Holes Filled with Magnetic Fluid into a Terbium Gallium Garnet Fiber. *IEEE Trans. Magn.* **2015**, *51*, 1–4. [[CrossRef](#)]
31. Hong, C.Y.; Yang, S.Y.; Horng, H.E.; Yang, H.C. Control parameters for the tunable refractive index of magnetic fluid films. *J. Appl. Phys.* **2003**, *94*, 3849–3852. [[CrossRef](#)]
32. Wang, J.; Pei, L.; Weng, S.; Wu, L.; Huang, L.; Ning, T.; Li, J. A Tunable Polarization Beam Splitter Based on Magnetic Fluids-Filled Dual-Core Photonic Crystal Fiber. *IEEE Photonics J.* **2017**, *9*, 1–10. [[CrossRef](#)]
33. Li, J.; Wang, R.; Wang, J.; Zhang, B.; Xu, Z.; Wang, H. Novel magnetic field sensor based on magnetic fluids infiltrated dual-core photonic crystal fibers. *Opt. Fiber Technol.* **2014**, *20*, 100–105. [[CrossRef](#)]
34. Riesen, N.; Love, J.D. Ultra-Broadband Tapered Mode-Selective Couplers for Few-Mode Optical Fiber Networks. *IEEE Photonics Technol. Lett.* **2013**, *25*, 2501–2504. [[CrossRef](#)]
35. Yang, Y.; Chen, K.; Jin, W.; Chiang, K.S. Widely Wavelength-Tunable Mode Converter Based on Polymer Waveguide Grating. *IEEE Photonics Technol. Lett.* **2015**, *27*, 1985–1988. [[CrossRef](#)]
36. Li, X.; Sun, B.; Yu, Y. Ultra-wide bandwidth wavelength selective couplers based on the all solid multi-core Ge-doped fibre. *Opto-Electron. Rev.* **2014**, *22*, 166–170. [[CrossRef](#)]

